Development of laser-optical measurement techniques on the vortex tube: Taking PIV to its limits

Eike J. Burow*, Ulrich Doll, Joachim Klinner, Guido Stockhausen, Christian Willert

Institute of Propulsion Technology, German Aerospace Center (DLR), Germany

* Correspondent author: eike.burow@dlr.de

Keywords: PIV, vortex tube, reference experiment, development platform

ABSTRACT

The Ranque-Hilsch vortex tube (RHVT) is referred to as one of the unsolved problems in physics: consisting of a cylindrical tube with several tangential inlet nozzles only, the expanded gas forms a complex internal flow field, resulting in a unique temperature separation effect. Since the vortex tube's invention by Ranque (1933) and Hilsch (1947) it has been used for decentralized cooling and gas cleaning purposes. While so far it has been investigated by means of conventional probes as well as laser-optical techniques such as FRS, L2F and LDA, this contribution targets on planar two-component PIV measurements. While the usual configuration features one outlet on each end of the tube, it will be shown that the major internal flow phenomena occur in a similar manner on a uni-flow configuration with only one outlet opposite to the inlet. The focus however is not on the temperature separation. Instead the RHVT is introduced as a development platform for laser-optical methods: it will be shown that the RHVT's complex flow topology is pushing the PIV technique to its limits; challenges and possible solutions are discussed. Especially the high tangential velocity component results in a strong projection error in the observed axial and radial velocities: to address this issue stereoscopic PIV will be deployed for the purpose of mapping the RHVT.

1. Introduction

Application-oriented development of laser-optical measurement techniques in laboratory environments often lacks the complex characteristics of realistic technical flows. Measurement campaigns on test rigs on the other hand usually offer very limited space for developing and testing laser-optical measurement techniques. The Ranque-Hilsch vortex tube (RHVT) with its simple geometry but nevertheless complex flow features has been proven to be an effective tool to close this gap (Doll, 2015). As shown in Fig. 1 (top) the device has no moving parts and consists of a tube made of glass with tangential inlet nozzles for pressurized gas on the left end. In the presented uni-flow configuration the process gas streams through the tube towards the single outlet on the right with decreasing vorticity, forming secondary structures such as a counter-flow along the tube axis and several vortex systems (Xue, 2010). A visualization of Mie-scattered light (Fig. 1, bottom) gives a first impression of the effects on the seeding particle distribution.
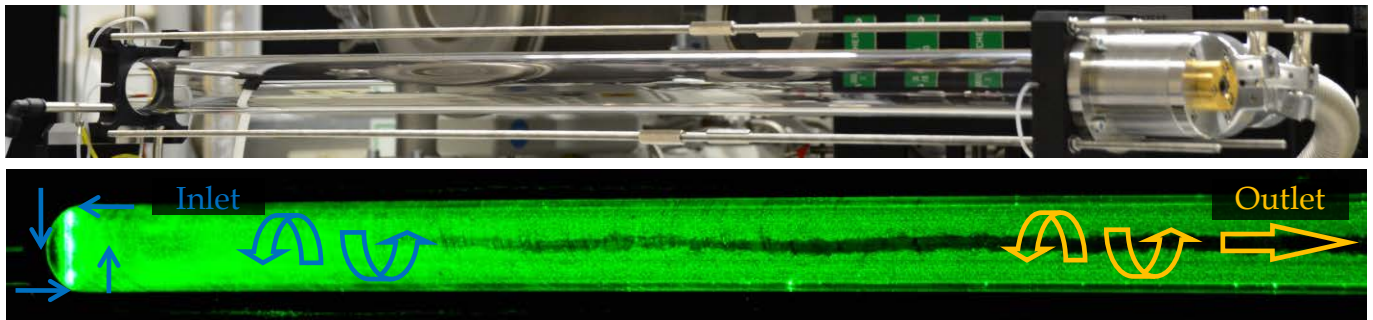
Fig. 1: Although the vortex tube (top) features no moving parts whatsoever a complex flow geometry is formed as indicated by scattered light from seeded particles (bottom).

The RHVT was first described by Ranque (1933) and Hilsch (1947). They discovered a unique temperature separation process: if a second partial outlet is added centrically at the left end as found in their original design, then separate cold and hot gas streams can be extracted. While the used uni-flow RHVT with a single outlet does not offer the possibility to extract heated and cooled gas streams from the system, still the major internal mechanisms are expected to be similar: uni-flow vortex tubes with two outlets on the right end on different radii were found to produce a strong temperature separation as well (Eiamsa-ard, 2008).

Since its invention the RHVT is commonly used for decentralized cooling and industrial gas cleaning. The internal temperature separation itself has been the focus of multiple research endeavors and several theories attempt to explain the apparent occurrence of "Maxwell's demon" (Liew, 2012). While the second law of thermodynamics remains unchallenged there currently is no consensus about the internal redistribution processes. Popular theories include acoustic streaming (Kurosaka, 1982 a), multi-circulation (Xue, 2013) or compression and expansion along the radial pressure gradient due to secondary circulations ('heat pump effect', Liew 2012).

In order to gain insight into the underlying mechanisms of the temperature separation process, information on the flow field as well as the thermodynamic properties inside the vortex tube is needed (Gao, 2005). Numerical simulations are capable of grasping partial aspects of the system but struggle to capture the flow phenomena as a whole (Morsbach, 2015). Most experimental investigations found in the literature rely on conventional probe-based technology (Hansske, 2011; Xue, 2013). Contact-free pointwise velocity measurements have been performed by means of Laser/Phase Doppler Anemometry (LDA/PDA: Liew, 2013) and Laser-2-Focus (L2F: Doll, 2014). Planar temperature and 1c-velocity measurements with Filtered Rayleigh Scattering (FRS) are in general agreement with recent probe-based results (Doll, 2015; Hansske, 2011).

The aim of this contribution is to introduce the RHVT as a development platform for laser-optical measurement techniques in general; especially endoscopic applications of FRS, Particle Image Velocimetry (PIV), L2F and Doppler Global Velocimetry (DGV) are expected to benefit from the complex laboratory experiment. Within this contribution first results and experiences with planar two-dimensional PIV on the RHVT will be presented. While the results still suffer from systematic errors and are thus considered to be work in progress, they demonstrate the vortex tube's ability to take measurement techniques to their limits.

2. Experimental setup and data evaluation

A schematic of the experimental setup is given in Fig. 2. The Vortex tube is set up in a uni-flow configuration with only one outlet on the right side. The inlet is designed as four tangential inlet nozzles with a diameter of 1.5 mm each. The inlet plane, also referred to as the vortex chamber, marks $x = 0$. At $x = -4.2$ mm the left end of the RHVT is sealed by a window. To achieve radial symmetry the outlet on the right end is designed as a circular slit formed by the tube and a cone. This slit intends to decouple the vortex tube from any asymmetry of the downstream settling chamber. Closed loop operation allows the use of different gases such as helium (He) or sulfur hexafluoride (SF_6) for a variation of relevant dimensionless numbers such as the Reynolds number (Körner, 2010). Since at this point the flow features themselves are of secondary interest only one operating condition is applied. Data were acquired for air and SF_6. Tracer particles consist of pure paraffin oil to avoid a contamination of the process gas with ethanol that is normally used in a mixture with paraffin to achieve smaller droplets after atomization.

The light sheet spans the entire tube diameter across the central plane and is introduced through the window on the left in Fig. 2. Both window and tube are antireflective coated for 532 nm. Due to the high out-of-plane velocity component (the tangential velocity is expected to be at least 5 times the axial and radial velocities) a combination of a short pulse distance and relatively high light sheet thickness is required. The beam waist is designed as such that the entire tube is within its Rayleigh length with a waist size between 0.8 and 1.1 mm. Pulse distances of 1 µs for air and 2 µs for SF_6 were found to be sufficient to capture the flow with a minimum of 60% matched particle pairs in critical areas. However with a field of (FOV) view spanning the entire tube diameter and a magnification of 62.7 pix/mm, the observed particle shift is below 2 pix in most areas. PIV images are captured by an interline CCD camera aligned orthogonally to the light sheet. An additional camera under an observation angle of 30° was set up to enable stereoscopic measurements. In this configuration the absolute measurement uncertainty of the tangential

component is expected to be about three times the axial and radial uncertainty (Westerweel, 2000) resulting in similar relative uncertainties.

Particle image interrogation (Willert, 1991; Raffel, 1998) is conducted with the commercial software PIVview (PIVTEC GmbH). Image preprocessing includes background subtraction – mean of 25 images without seeding – followed by dynamic histogram clipping to include particles of reduced intensity in the correlation (Shavit, 2007). Image contrast is further enhanced by a Gaussian high pass filter. Interrogation areas span (48 pix)² with a 33% overlap and typically contain 5-20 particle images. Outlier detection is based on a normalized median test (Westerweel, 2005) and a minimum correlation value. While for each field of view 175 measurements are performed, the summarized valid correlation value of each interrogation area Σc_v is again checked against a minimum value to exclude erroneous vectors from regions of low tracer density (see Fig. 1). With a field of view spanning 31.6 mm and a traversing distance of 25 mm the overlapping data is optionally linearly interpolated.
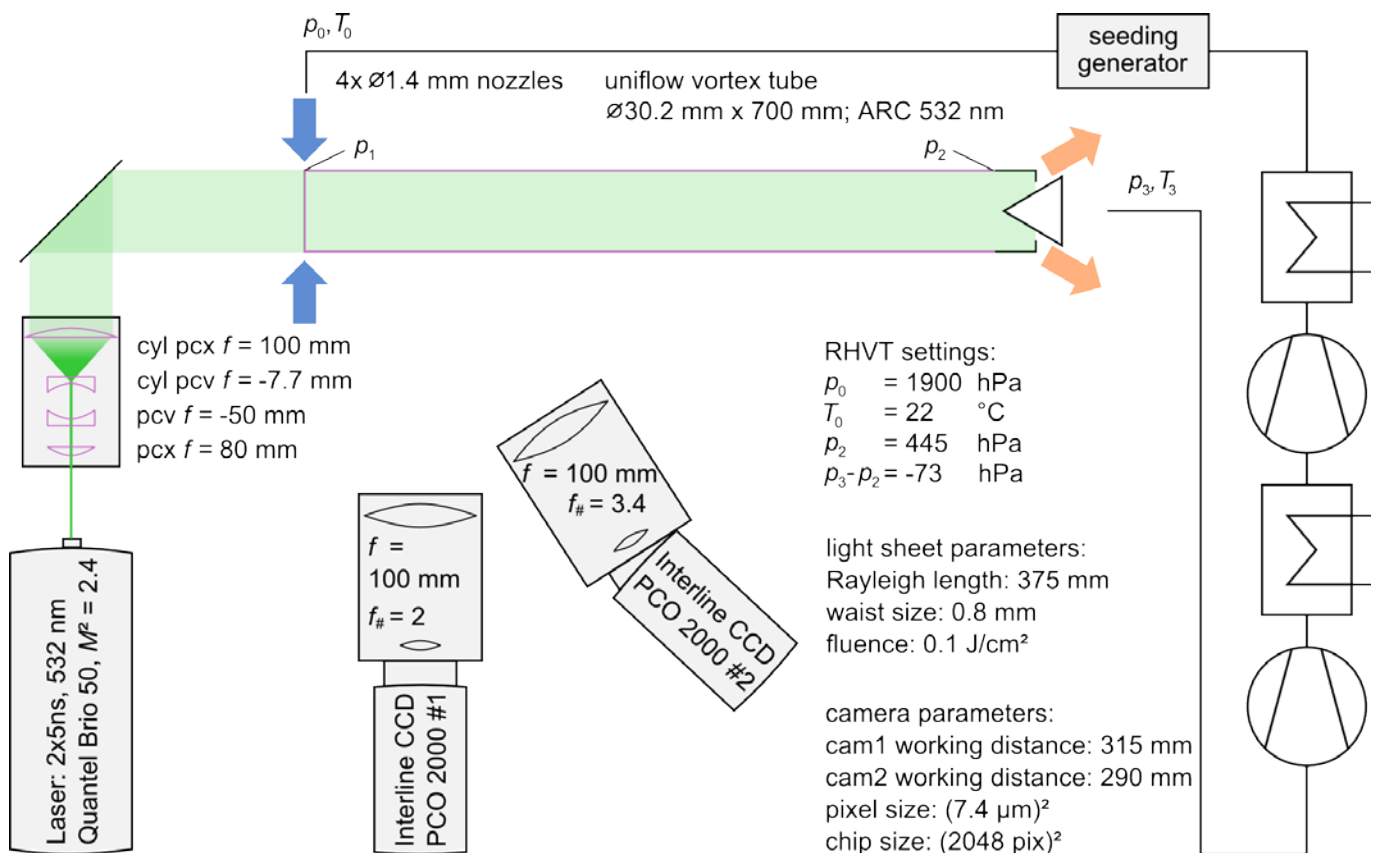

Fig. 2: Schematic of the measurement setup with key parameters and operating conditions.

3. Measurement results

Time averaged measurement results are shown in Fig. 3 (air) and Fig. 4 (SF₆). From top to bottom each data set consists of: axial velocity u_x, radial velocity u_y, vorticity $\omega_z = \partial u_y/\partial x - \partial u_x/\partial y$ and the ensemble correlation value Σc_v.
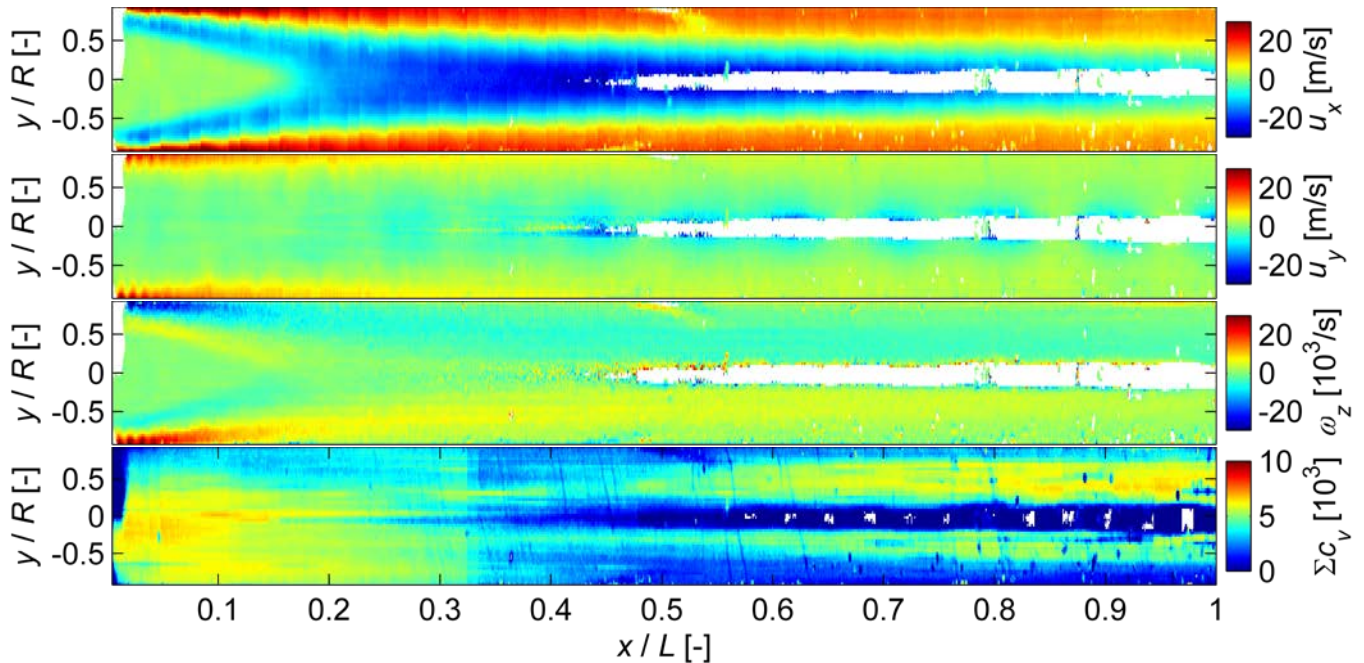

Fig. 3: An overview of time averaged PIV results in air is presented in the following order (top to bottom): axial velocity, radial velocity and vorticity; the ensemble correlation value serves as a data quality index.
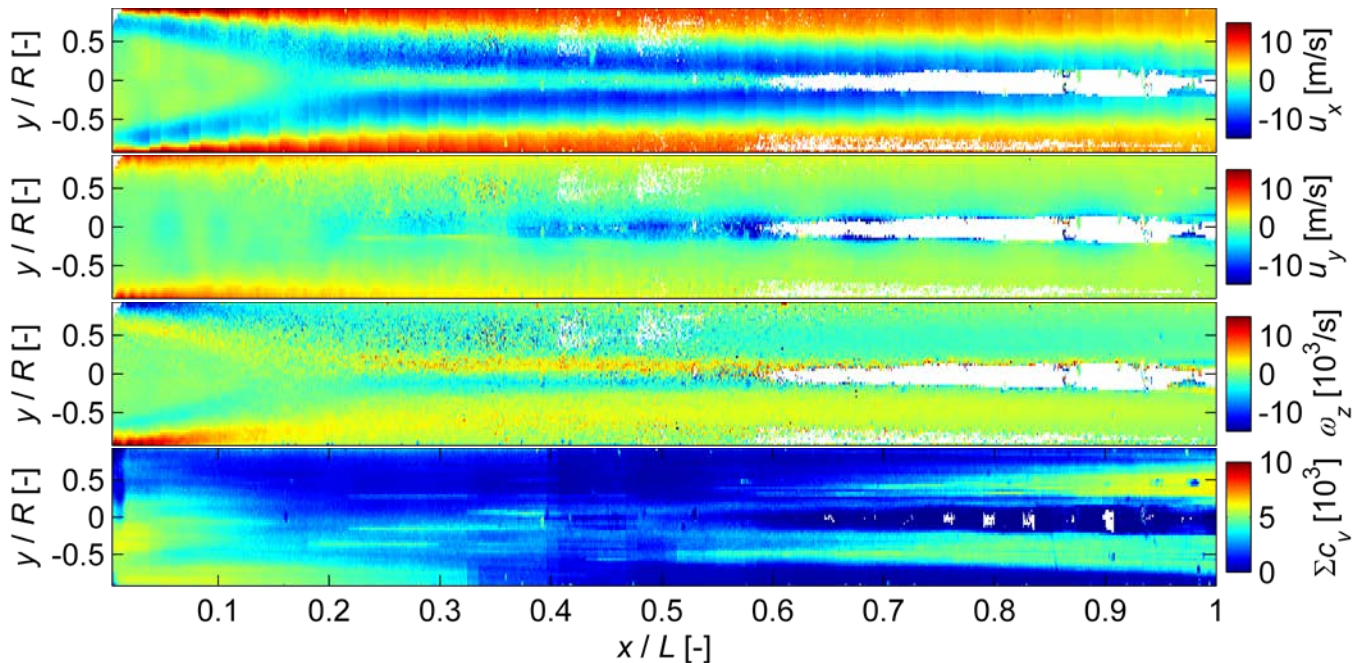

Fig. 4: Time averaged results in SF₆ are presented in the same manner as in Fig. 3.

Although systematic errors and sources of uncertainty will be discussed later the impact of projection errors are briefly discussed here. While the axial velocity profiles are only affected quantitatively (ref. section 4) the radial velocity exhibits a strong positive offset close to the wall: the flow appears to be strongly directed upwards on both sides, although the wall shear layer would not allow for a high positive vertical velocity in the area – this is obviously an artifact. Fortunately projection errors are restricted to ∇u, but the vorticity $\nabla \times u$ is barely affected; thus it will be frequently referred to in this section.

Regarding the results in both air and SF_6, the tube can be divided into three sections: small-scale instabilities up to $x/L \approx 0.05$, a conical transition area to the left up to $x/L \approx 0.15$ and a circulation area covering the majority of the tube length. While SF_6 and air were measured under the same operating conditions as summarized in Fig. 2 the SF_6 measurements feature about 50% the Reynolds number and 40% the molar flux. Thus it is not surprising that velocities and vorticity are reduced to 50% in comparison to the measurements in air. However, driven by the higher molar mass of SF_6 the measured pressure reduction $p_2 - p_1$ between the inlet and outlet plane is about 15% higher (60 hPa in SF_6 compared to 52 hPa in air). For the most part however the flow structure is consistent between the two gases.

Due to constructive constraints the inlet plane itself could not be measured; nonetheless small-scale instabilities directly following the vortex chambers are visible within the first field of view, starting 4.5 mm downstream (as seen enlarged in Fig. 5 for air). The localized small-scale swirls occur periodically, about 7.5 mm apart – corresponding to a sonic frequency of 46 kHz – and dissipate quickly in favor of a homogeneous high-vorticity layer close to the wall. This area already shows an influence of the macroscopic counter-flow driven by mechanisms far downstream: the positive angular momentum close to the wall and the neutral cone in the center are separated by a region of low negative angular momentum.
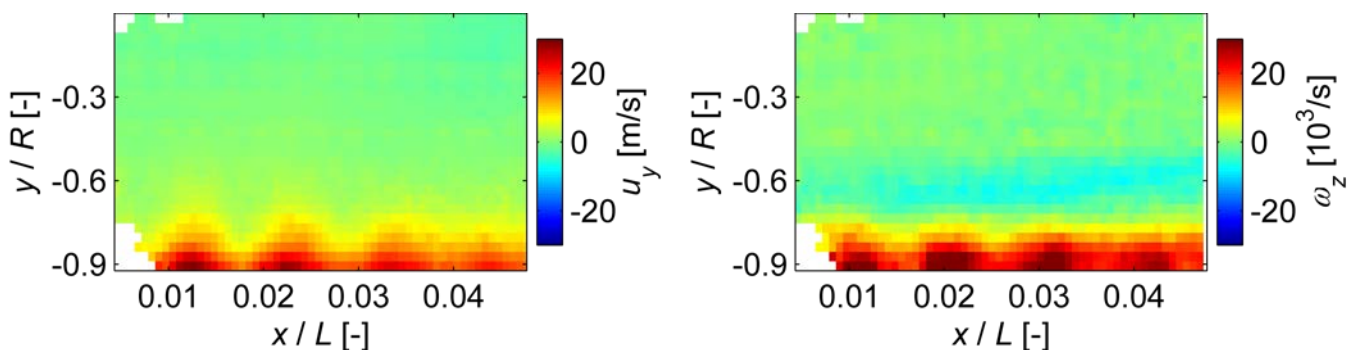

Fig. 5: At the vortex chamber – near the inlet nozzles and close to the wall – the flow field exhibits the highest turbulence within the smallest scales. Although the level of u_y (left) is strongly falsified by a projection error the periodicity is well visible. The correct vorticity data (right) shows the beginning influence of the counter-flow.
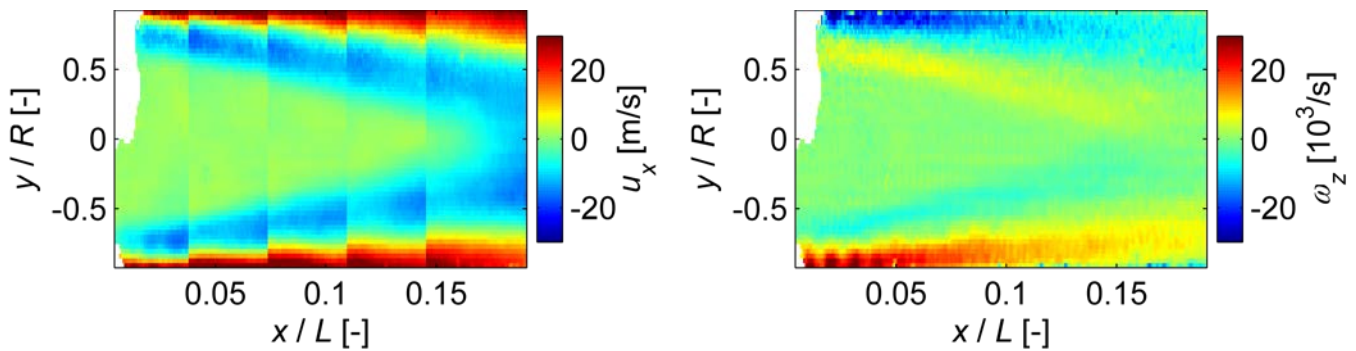
Fig. 6 - Axial velocity (left; no linear interpolation) and vorticity (right) in air: Within the transition area small scale inlet jets from the vortex chamber transform into macroscopic structures spanning the entire tube.

This becomes more obvious when looking at the mean axial velocity field in the transition area (Fig. 6, left). Up to $x/L = 0.15$ the flow topology features a conical area with negligible axial and radial velocities. Preliminary results from stereoscopic PIV measurements indicate that tangential velocities are dominated by a solid body rotation. Negative axial velocities between this cone and the major mass transport near the wall represent the stable and significant counter-flow. Aside from effects of the turbulent shear layer the sign change in the vorticity data also indicates vortices that may contribute to the temperature separation effect by a multi-circulation as described by Xue (2013). In this section however the vortices themselves are delocalized; the complete circular character can only be observed in single shot images (Fig. 10).

The majority of the tube from $x/L = 0.3...1$ is governed by negative axial velocities in the center and positive axial velocities near the tube's boundaries, with the radius of zero velocity decreasing towards the outlet on the right (Fig. 3, top). The only qualitative difference between air and SF_6 occurs here: while air as process gas demonstrates a consistent counter-flow, the SF_6 data show zero axial velocity right at the tube's center, within the counter-flow (Fig. 4, top). Kurosaka explained the temperature separation on uni-flow vortex tubes (and the lack of differences to the bidirectional setup) with a predominant influence of radial effects (Kurosaka, 1982 b), now it can be seen that this is not necessarily the case since the axial counter-current can occur as well. Compared to data from FRS measurements on a bidirectional RHVT of the same dimensions (Doll, 2015) the quantitative differences are within what can be expected from different operating conditions.

Tangential velocities – again as preliminary results from stereoscopic measurements – do not appear to follow a solid body rotation and deserve a closer look in the future. Radial velocity data (Fig. 7, air) close to the wall should be disregarded at this point again due to the projection error – data on the axis on the other hand are limited due to poor seeding density as indicated by

Fig. 1 (bottom). The area in between however – ranging from $y/R = 0.15...0.45$ – shows a periodic sign change in the radial velocity data indicating localized vortices. This also agrees well with previously reported data (Doll, 2015) and supports separation mechanisms such as multi-circulation (Xue, 2013) and heat pump effects (Liew, 2012). While the visualization of acoustic effects via PIV is challenging it still can be said that the periodicity of this vortex system corresponds to a sonic frequency around 5 kHz. When Kurosaka formulated the temperature separation by acoustic streaming he found the first harmonic resonance to be in the same order of magnitude (Kurosaka, 1982 a).
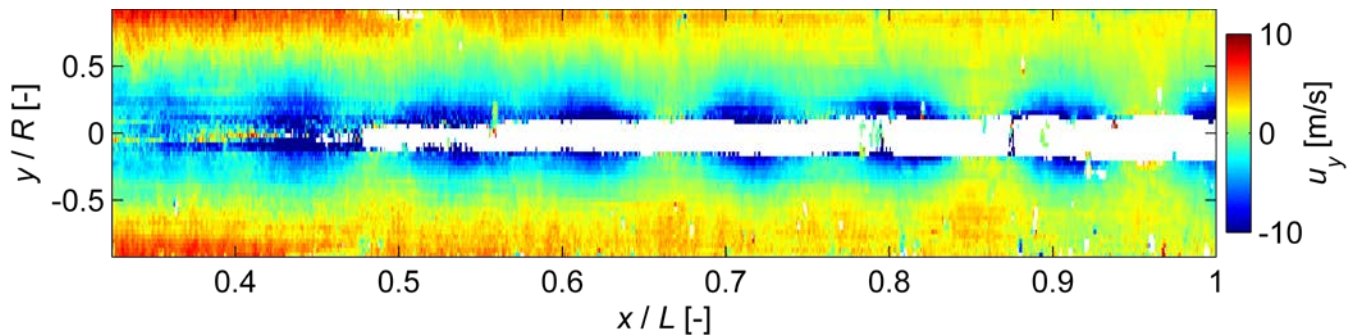

Fig. 7: The radial velocity shows periodic sign changes in the center of the tube indicating localized vortices.

4 Discussion

The presented PIV results illustrate several limitations to the measurement technique. One of them is its dependency on seeding particles: while the seeding distribution is homogeneous up to $x/L \approx 0.15$ – corresponding to the transition area – further downstream the recirculating gas in the tube's center carries diminishing amounts of particles (Fig. 8). As a result reliable time-averaged data on the axis can only be provided up to $x/L \approx 0.45$ in air and $x/L \approx 0.6$ in SF6 (Fig. 3,4; top). Any valid correlations beyond that point are based on rare occurrences of single particle formations crossing through the counter-current. These data represent a sampling of a special type of event and cannot be used for interpretation of the mean flow (conditional sampling).
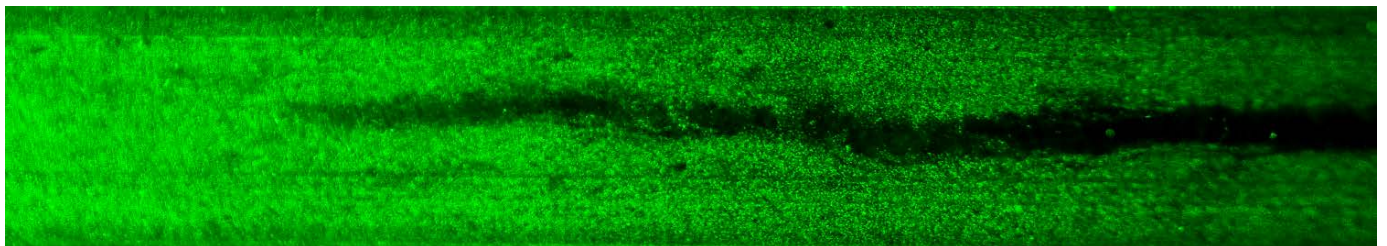

Fig. 8: Single shot Mie scattering image of particles inside the vortex tube
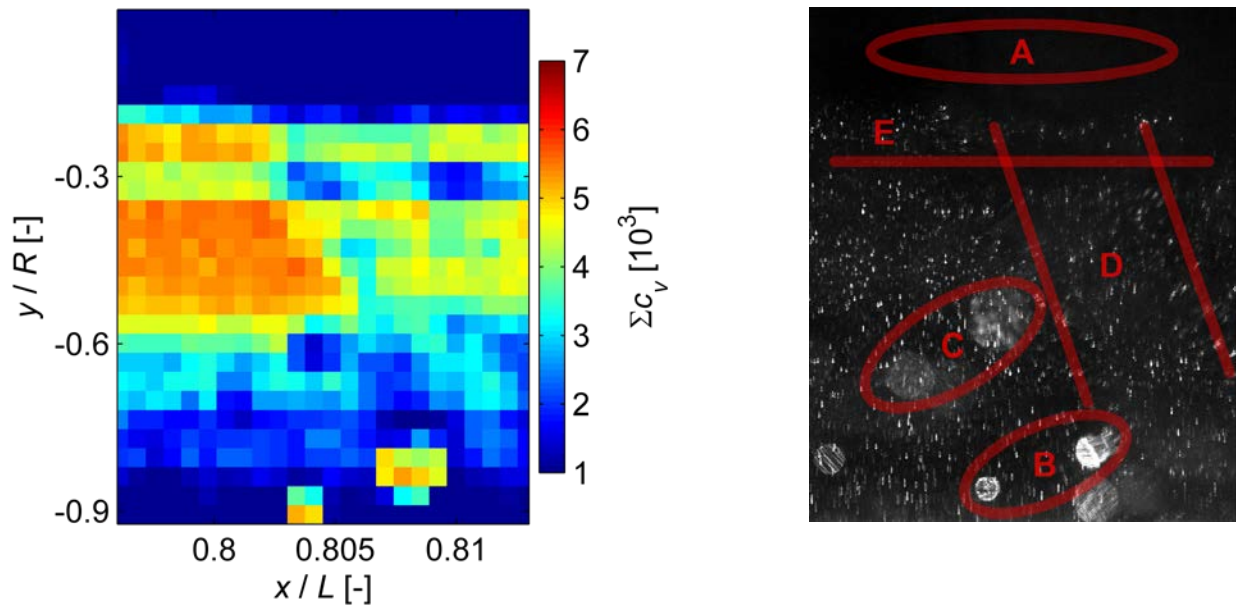
Fig. 9: Most disturbances in seeding density, lighting and imaging result in low correlation values; some stains however produce seemingly reliable artifacts.

Fortunately correlation values are correspondingly low in these cases so the false information can be easily omitted: Fig. 9 depicts a critically disturbed area of a single shot image (right) with the corresponding particle cross-correlation coefficient (left), the seeding-free tube axis is marked as 'A'.

Seeding also tends to accumulate on the wall, leaving large und thus bright drops on the surface. Although they are far outside of the depth of focus, some are still bright enough to dominate the PIV correlation ('B'): the result is a relatively high correlation value with zero measured velocity. Most drops are imaged sufficiently diffuse such that actual particle images in the flow can be seen behind them nonetheless – this results in valid PIV evaluations with a reduced correlation value due to the additional background ('C'). Over time these drops also tend to accumulate and move along the surface flow's streamlines. Like rain drops on a window seeding drops repeatedly move within the same tracks leaving behind an oil film which blurs particle images in the area ('D'). While the correlation value is reduced (Fig. 3, bottom, shows several of these diagonal stripes) the final data are not severely affected. Over time seeding also precipitates and forms drops on the window used to introduce the light sheet: their shadows can be seen as horizontal darkened areas ('E'). Since light intensity is not a limiting condition here, the correlation value is again reduced but still sufficient. Seeding residue on the window also leads to a significant background in the proximity, thus PIV evaluations on the left end of the tube are limited (e.g. the unmapped area in the top left corner of Fig 6).
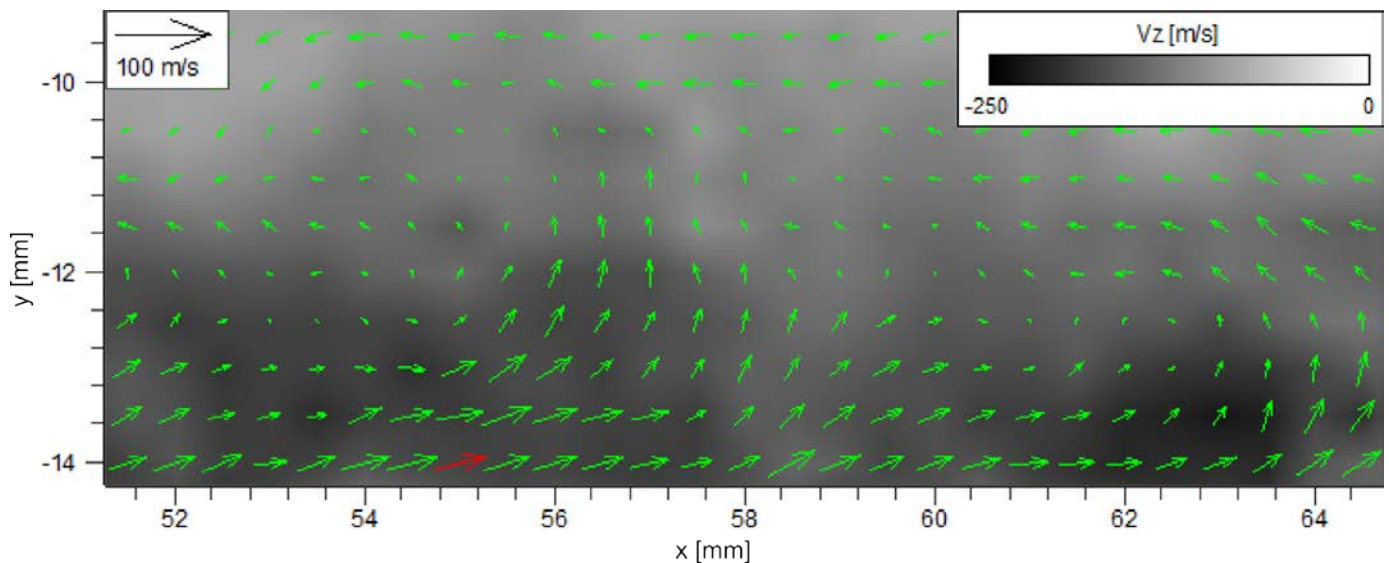
Fig. 10: Preliminary stereoscopic measurements correct for the camera observation geometry but still suffer from a projection error due to the distortion by the glass cylinder.

While any effects of imaged stains can be reduced by opening the lens aperture and thereby reducing the depth of focus, this also leads to increased particle image distortions. This is especially the case for distortions introduced by the glass tube itself: while particles observed through the tube vertically (close to the tube's center; top of Fig. 9, right) appear as circular dots with a maximum diameter of 5 pixels, particles close to the wall basically exhibit a significant astigmatism and appear as ~16 pixels long vertical streaks (bottom of Fig. 9, right). In consequence the measurement uncertainty in the radial velocity is strongly increased. Furthermore the reduced SNR leads to an additional isotropic increase in the measurement uncertainty. The trade-off between stain drop circumvention and particle imaging quality is a matter of trial-and-error requiring a compromise for each setup.

More serious than particle image blurring and distortion however is the change in the observation angle. When looking through an idealized pinhole camera only the center pixel is observed vertically. The further a pixel is distanced from the center the more the observed coordinate system (CS) is tilted: in-plane and out-of-plane velocity deviate from the experiment's CS – in this case referred to by axial, radial and tangential directions. Disregarding the observed CS this effect can be interpreted as a cross-talk of the out-of-plane component on the planar 2C-data. It is apparent that without additional information this systematic error cannot be eliminated. With the RHVT's complex flow topology any simplified assumption on the out-of-plane component such as global linear solid-body-rotation is invalid. The effect of this projection error can be seen on Fig. 6 (left): the fields of view do not seem to align; especially in the outer

region (highest u_z and largest observation angle) each FOV suffers from a more or less linear cross-talk from left to right $\partial u_x(x, u_z(y))/\partial x$.

One possible solution is the simultaneous measurement of all three components via stereoscopic measurements; with a suitable mapping the velocity can be transformed to the original CS from two particle images under different observation angles, assuming a common projection center for each entire image. Fig. 10 shows a resulting single shot image. While the camera's CS can be corrected, a second change in the (vertical) observation angle is introduced by the distortion of the glass tube: the radial velocity data still show an offset $\partial u_y(y, u_z(y))/\partial y$ in the same order of magnitude as the data itself.
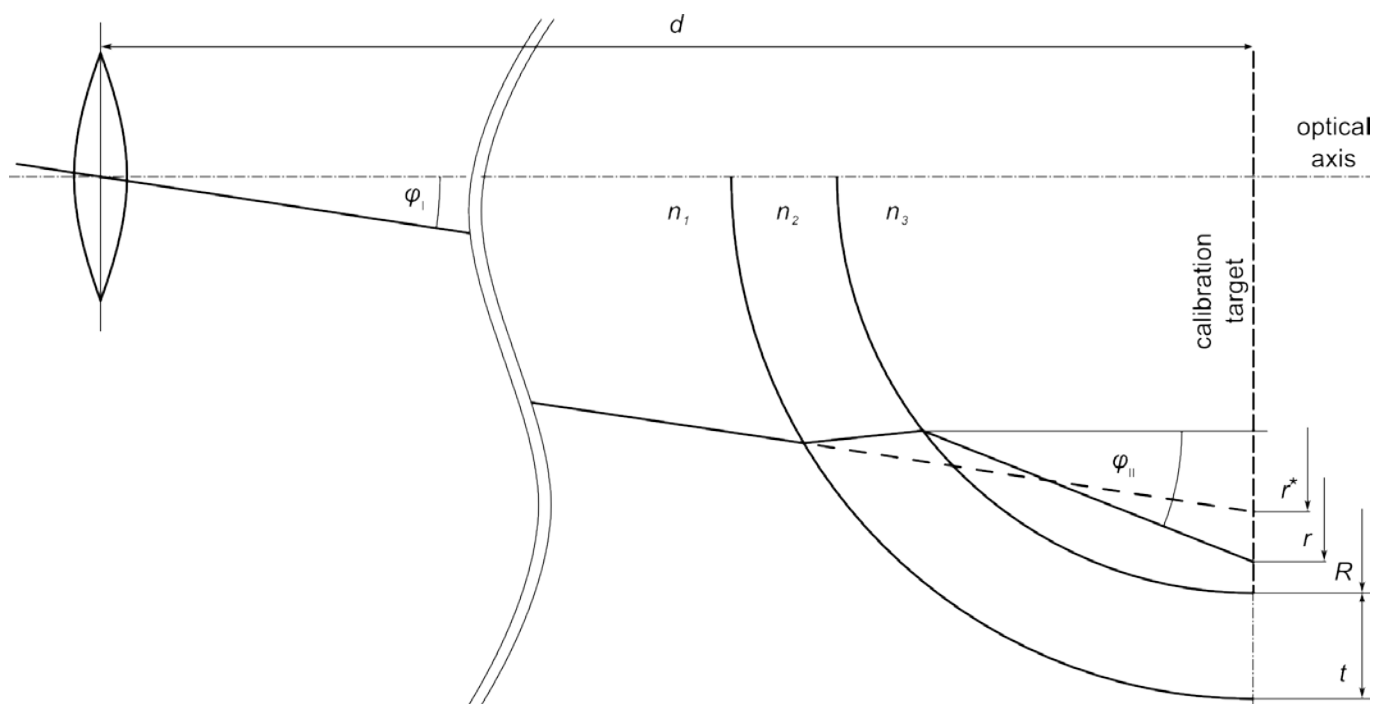

Fig. 11: Due to the curved glass surface the image no longer has a common projection center.

Figure 11 demonstrates the refraction on the curved glass surface in a simplified planar manner. Target mapping can account for a pixel's camera view angle φ_I and the distortion leading to the difference between the observed radius r^* and the object radius r. The coordinate system's total tilt however is found in the local view angle φ_{II}. Besides the camera distance d and the camera view angle φ_I it depends on the tube dimensions R and t as well as the relevant refractive indices n_i. Including this additional information into the stereo PIV evaluation is currently work in progress.

5 Conclusion

The flow topology within a Ranque-Hilsch vortex tube was characterized two-dimensionally in high resolution via particle image velocimetry. While the vortex tube serves a purpose on its own, in this context it provides the development platform for laser-optical measurement techniques, thus it is set up for maximal optical access and a variety of possible operating conditions. Using it as a reference experiment for upcoming conventional and endoscopic work on Filtered Rayleigh Scattering, Doppler Global Velocimetry and Laser-2-Focus as well, PIV measurements are intended to serve as a reference: out of the mentioned techniques PIV is most suitable to deliver an overview on the flow field.

Due to the flow characteristics inherent to the vortex tube however the data are still corrupted by systematic errors, especially a projection error resulting in a cross-talk of the high tangential velocity on the measured axial and radial velocity. Thus the work on the PIV application to the RHVT is far from completed: an adapted stereoscopic approach is supposed to deliver three-dimensional data; FRS and DGV velocity data evaluation are also expected to profit from the extended model. Also since so far only one operating condition has been measured, the behavior of key flow dimensions under changing conditions will be examined further; a direct comparison of the presented uni-flow configuration to a bidirectional setup also deserves another look to gain further insight into the working mechanisms of the RHVT.

References

Doll U, Beversdorff M, Stockhausen G, Willert C, Schlüß D, Morsbach C (2014) Characterization of the flow field inside a Ranque-Hilsch vortex tube using filtered Rayleigh scattering, Laser-2-Focus velocimetry and numerical methods. 17th Lisbon Symposium.

Doll U, Burow E J, Beversdorff M, Stockhausen G, Willert C et al (2015) The Flow Field inside a Ranque-Hilsch Vortex Tube Part I: Experimental Analysis using Planar Filtered Rayleigh Scattering. The 9th Symposium on Turbulence and Shear Flow Phenomena, Melbourne.

Eiamsa-ard S, Promvonge P (2008) Review of Ranque-Hilsch effects in vortex tubes. Renewable and sustainable energy reviews 12 (7):1822-1842.

Gao C, Bosschaart K, Zeegers J, de Waele A (2005). Experimental study on a simple Ranque-Hilsch vortex tube. Cryogenics 45:173-183.

Hansske A, Ziegler F (2011) Experimental investigation of a vortex tube. 23rd IIR international Congress of Refrigeration, Prague.

Hilsch R (1947) The Use of the Expansion of Gases in a Centrifugal Field as Cooling Process. Review of Scientific Instruments 18 (2):108-113.

Körner M, Resagk C, Thess A (2010) Experimental investigation of non-isothermal indoor airflow in a small-scale model room using LASER techniques. 15th International Symposium on Applications of Laser Techniques to Fluid Mechanics, Lisbon.

Kurosaka M (1982 a) Acoustic streaming in swirling flow and the Ranque-Hilsch (vortex-tube) effect. J. Fluid Mech. 124:139-172.

Kurosaka M, Chu J Q, Goodman J R (1982 b) Ranque-Hilsch Effect Revisited: Temperature Separation Traced to Orderly Spinning Waves or 'Vortex Whistle'. AIAA/ASME 3rd Joint Thermophysics, Fluids, Plasma and Heat Transfer Conference, St. Louis.

Liew R, Zeegers J C H, Kuerten J G M, Michalek W R (2012) Maxwell's demon in the Ranque-Hilsch vortex tube. Physical Review Letters 109, 054503.

Liew R, Zeegers J, Kuerten J (2013) 3D Velocimetry and droplet sizing in the Ranque–Hilsch vortex tube. Experiments in Fluids 54, 1416.

Morsbach C, Schlüß D, Franke M et al (2015) The Flow Field inside a Ranque-Hilsch Vortex Tube Part II: Turbulence Modelling and Numerical Simulation. The 9th Symposium on Turbulence and Shear Flow Phenomena, Melbourne.

Raffel M, Willert C E, Kompenhans J (1998) Particle Image Velocimetry - A Practical Guide. Springer, Berlin Heidelberg.

Ranque G J (1933) Experiments on expansion in a vortex with simultaneous exhaust of hot air and cold air. Le Journal de Physique et le Radium 115 (4):112–114.

Shavit U, Lowe RJ, Steinbuck JV (2007) Intensity Capping: a simple method to improve cross-correlation PIV results. Experiments in Fluids 42(2): 225-240.

Westerweel J, van Oord J (2000) Stereoscopic PIV measurements in a turbulent boundary layer. Stanislas M, Kompenhans J, Westerweel J (eds) Particle Image Velocimetry: Progress toward Industrial Application. Kluwer, Dordrecht, pp 459-478.

Westerweel J, Scarano F (2005) Universal outlier detection for PIV data. Experiments in Fluids 39(6): 1096-1100.

Willert C E, Gharib M (1991) Digital particle image velocimetry. Experiments in Fluids 10 (4):181-193.

Xue Y, Arjomandi M, Kelso R (2010) A critical review of temperature separation in a vortex tube. Experimental Thermal and Fluid Science 34 (8):1367-1374.

Xue Y, Arjomandi M, Kelso R (2013) The working principle of a vortex tube. International Journal of Refrigeration, 36:1730-1740.